Global Biogeochemical Cycles®

RESEARCH ARTICLE
10.1029/2021GB007268

Special Section:
The Arctic: An AGU Joint Special Collection

The Pan-Arctic Continental Slope as an Intensifying Conveyer Belt for Nutrients in the Central Arctic Ocean (1985–2015)

L. Oziel[1], V. Schourup-Kristensen[2], C. Wekerle[1], and J. Hauck[1]

[1]Alfred-Wegener-Institut Helmholtz-Zentrum für Polar- und Meeresforschung, Bremerhaven, Germany, [2]Department of Ecoscience, Aarhus University, Roskilde, Denmark

Key Points:

- The pan-Arctic continental slope contributes disproportionately to the transport of nutrients in the Central Arctic Ocean (CAO)
- The nutrient supply intensifies along the slope through upwelling and lateral eddy transport but decreases in the interior basins
- Despite an intensification of ocean dynamics, the CAO is still shifting from a light-limited to a nutrient-limited system

Supporting Information:

Supporting Information may be found in the online version of this article.

Correspondence to:

L. Oziel,
laurent.oziel@awi.de

Citation:

Oziel, L., Schourup-Kristensen, V., Wekerle, C., & Hauck, J. (2022). The pan-Arctic continental slope as an intensifying conveyer belt for nutrients in the central Arctic Ocean (1985–2015). *Global Biogeochemical Cycles*, *36*, e2021GB007268. https://doi.org/10.1029/2021GB007268

Received 7 DEC 2021
Accepted 18 MAY 2022

Abstract Primary production in the Central Arctic Ocean (CAO) is limited by light and bioavailable nutrients. With the decline of the sea-ice cover in recent decades, and the resulting increase in light availability, nitrate limitation has been speculated to become more prominent. We used an eddy-permitting biogeochemical model simulation to estimate nitrate advective fluxes at different spatio-temporal scales (synoptic, mesoscale and sub-mesoscale) over the 1985–2015 period. We found that the pan-Arctic continental slope contributes disproportionately to the Dissolved Inorganic Nitrogen supply and that this supply is intensifying through two main processes: lateral eddy transport and upwelling. Despite this increasing supply in nitrate and an intensification of ocean dynamics, the nutrient supply is decreasing everywhere else in the central basins and the simulation indicates that the CAO is still shifting from light to nutrient limitation.

Plain Language Summary Microscopic algae called phytoplankton are the base of the trophic chain, sustaining the entire Arctic Ocean (AO) ecosystem. In the central parts of the AO, multi-year sea-ice used to limit transmission of light in the surface ocean and therefore control phytoplankton growth and primary productivity. However, the massive loss in sea-ice during the last 3 decades allowed more and more light to penetrate the water column, making nutrient availability the main bottom-up control of the AO productivity. A major part of the bio-available nutrients reaching the surface in the central AO are transported with ocean currents from the adjacent North Atlantic and Pacific and from deeper water masses. Using a biogeochemical model resolving processes at high spatial resolution, we were able to quantify the different transport pathways of nutrients with ocean currents and revealed that despite increasing supply along the anticlockwise flowing boundary current, the central AO is still running into more severe nutrient limitation.

1. Introduction

The approximately 50% reduction of sea-ice volume in the last three decades (Kwok, 2018; Serreze & Meier, 2019; Stroeve & Notz, 2018) is one of the most striking implications of global Climate Change. The loss of sea-ice causes more light to penetrate into the water column (Nicolaus et al., 2012) allowing for longer growing seasons and increased primary production (Arrigo et al., 2008, 2015). Climate change projections estimate a likely summer ice-free Arctic Ocean (AO) by ~2050 (Sigmond et al., 2018). Therefore, we can expect the northernmost part of the central Arctic Ocean (CAO) to generally move from a predominantly light-controlled (ice-covered) to a more nutrient-controlled (open water) system (Babin, 2020). Future Net Primary Production (NPP) levels would then rely on "new" nutrient supply to the photic layer.

Without the physical entrainment of nutrients in the sunlit ocean, phytoplankton growth would be almost impossible. Future productivity will be impacted by the balance between (wind-driven) turbulence and buoyancy fluxes that control the AO circulation and stratification (Timmermans & Marshall, 2020). The traditional paradigm for the AO attributes increasing NPP to decreased stratification that increased the vertical supply of nutrients by diapycnal mixing. While larger open water areas will favor wind-driven turbulent mixing (Randelhoff et al., 2018) and upwelling (Arrigo et al., 2012; Spall et al., 2014) in some Arctic regions, the CAO exhibits very small convective winter replenishment (Codispoti et al., 2013) owing to weak turbulent mixing levels (Rainville et al., 2011). The diapycnal mixing rates are very low compared to the mid-latitude ice-free oceans (e.g., D'Asaro & Morison, 1992; Rainville & Winsor, 2008) or to seasonally stratified Arctic regions (Marginal Ice Zones such as the Barents Sea or Baffin Bay for instance; Randelhoff et al., 2020; Rippeth et al., 2015). The strong stratification in the CAO is explained by the existence of a perennial halocline as opposed to the Arctic shelves or in subpolar regions, where the halocline only forms seasonally in summer and where relatively strong

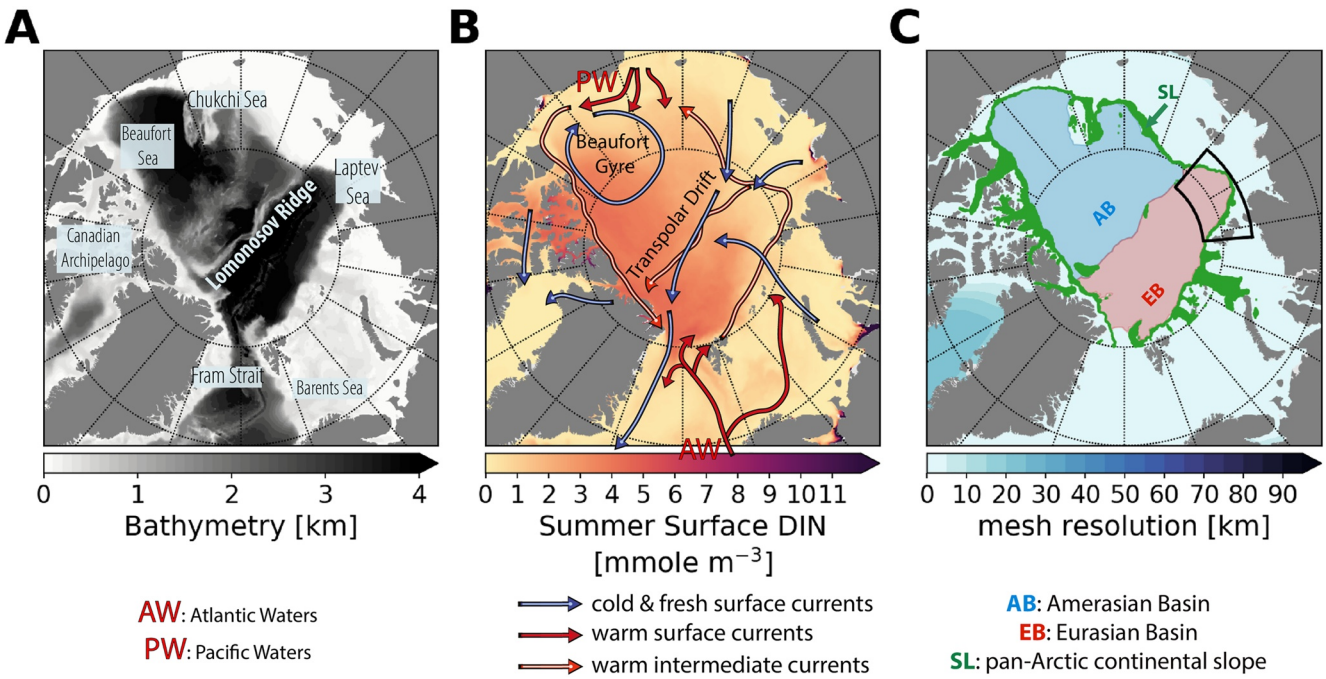

Figure 1. Arctic Ocean (a) Bathymetry; (b) September surface concentration for the 1985–2015 period with simplified circulation features. (c) Studied regions (Amerasian basin (AB)—in blue, Eurasian Basin (EB)—in red, pan-Arctic continental slope—SL—in green) with mesh resolution in background. The black frame in panel (c) indicates the eastern EB studied in Section 3.2 and Figure 5.

mixing can break down vertical stratification and homogenize the upper ocean during the winter (e.g., Randelhoff et al., 2015). The halocline separates the Surface Mixed Layer (SML), where primary production takes place, from nutrient-rich Atlantic Waters (AW) or Pacific Waters (PW) at intermediate depths. The CAO can therefore be considered as an advective ocean (Carmack & Wassmann, 2006; Hunt et al., 2016; Wassmann et al., 2015), through which nutrients are transported between the Pacific and Atlantic Oceans (Carmack et al., 2016; Popova et al., 2013; Yamamoto-Kawai et al., 2005) by the boundary currents flowing anticlockwise along the topographic slope (Figure 1b).

There is a long list of evidence that points toward rapid changes in the AO dynamics. It is urgent to quantify the levels and the evolution of advected nutrient supply in the CAO and impacts on primary producers. The CAO is not homogeneous and shows regional contrasted patterns of ocean dynamic changes (Brown et al., 2020) and can be divided into three regions (Figure 1c). Two distinct regions are the AB (extremely stratified, influenced by PW) and the Eurasian Basin (EB, moderately stratified, influenced by AW) (*sensu* E. Carmack & Wassmann, 2006). On the one hand, the EB experiences a phenomenon called "Atlantification" exacerbated by sea ice dynamics and subsequent feedback loops (Ingvaldsen et al., 2021). "Atlantification" comprises an increase in advection of temperate AW (Oziel et al., 2020; Qiang Wang, Wekerle, et al., 2020) and a decrease in stratification recently allowing winter ventilation events (Lind et al., 2018; Polyakov et al., 2017). On the other hand, freshwater tended to accumulate in the last decades in the AB, especially in the Beaufort gyre (e.g., Rabe et al., 2014), resulting in a stratification increase and a shift in the assemblage composition toward smaller phytoplankton (Li et al., 2009). As opposed to the EB, increasing stratification resulted in a scenario where ventilation is already no longer possible in the AB even with increased advective potential (Armitage et al., 2020; Woodgate & Peralta-Ferriz, 2021). Finally, one could also distinguish the pan-Arctic continental slope, a region of "sharp gradients of physical processes" (Bluhm et al., 2020). Here, a boundary ocean current sustains an intense circulation generating eddies (Crews et al., 2018; Mathis et al., 2007; Pnyushkov et al., 2018; Wang, Koldunov, et al., 2020), upwelling (Lin et al., 2019; Meneghello et al., 2018; Pickart et al., 2013; Sévigny et al., 2015), and vertical fluxes of nutrient and heat (Randelhoff et al., 2017; Schulz et al., 2021).

Recent advances therefore not only documented changes in the circulation but also in the mesoscale activity. A variety of recent observations and modeling experiments support the idea that (sub)mesoscale turbulence

influences phytoplankton growth by affecting both the nutrient and light environments (e.g., D'Ovidio et al., 2010; Lévy et al., 2018; Schourup-Kristensen et al., 2021; Tippenhauer et al., 2021). Nutrient supply occurring at the scale of eddies (the mesoscale) and at the scale of frontogenesis (the submesoscale) contribute significantly to the primary production budget (Lévy, 2008; Lévy et al., 2012). For a more exhaustive description of the role of (sub) mesoscale currents in structuring marine ecosystems, the reader can refer to the comprehensive review by Lévy et al. (2018). Here, we merely remind the reader of two key points:

1. **Mesoscale activity** such as geostrophic eddies are generated through barotropic and baroclinic instabilities of the mean currents that convert potential energy into kinetic energy. They dominate the eddy kinetic energy (EKE) of the ocean. Geostrophic eddies can regulate both the lateral and vertical transport of biomass and nutrients. They are closely linked to submesoscale motions.
2. **Submesoscale features** are generated through frontogenesis at the ocean surface (and other boundaries) that transfer energy from the larger scales. Frontogenesis occurs when large-scale currents or mesoscale eddies converge and bring together different water masses. Submesoscale motions are characterized by small vortices and a "mosaic" of rapidly changing small-scale density filaments and fronts. Because of their unstable nature, submesoscale fronts can generate intense vertical velocities that may transport nutrients from the deep pool into the euphotic zone, and phytoplankton into the dark. Horizontally, submesoscale motions are associated with stirring. Stirring alone only implies the redistribution of the biological constituents, which are transported by the currents, with no change in their concentrations. Thus, in principle, stirring alone should have no consequences on the productivity or diversity of marine ecosystems.

Eddy kinetic energy can contribute up to 70% of the total kinetic energy in some places of the CAO, and especially along the topographic slopes (Wang, Koldunov, et al., 2020). What are exactly the large-scale effects of (sub)mesoscale turbulence on nutrient dynamics, and therefore phytoplankton dynamics, in the CAO? How does (sub)mesoscale nutrient injection compare with the large basin-scale circulation supplies? How does horizontal supply compare with vertical supply? Can increasing fluxes alleviate increasing nutrient limitation?

In order to answer those questions, one should ideally focus on advective fluxes (not concentration) of nutrients to determine the long-term evolution of NPP since phytoplankton growth is a rate. In this study, we investigated Dissolved Inorganic Nitrogen (DIN), regarded as a primary constraining element for primary producers in the CAO (Tremblay et al., 2015). Major uncertainties remain in the evolution of the DIN fluxes in the Arctic leading to diverging projections of NPP at the end of the century (Vancoppenolle et al., 2013). The role for mesoscale and submesoscale advective processes have been largely overlooked in the total advective budget due to the lack of computer resources or fine-scale in situ sampling. At present, data are lacking to provide a quantitative, Arctic-wide assessment of temporal trends in nutrient advective fluxes. Eddy-permitting biogeochemical modeling is therefore a useful tool to assess this issue. In this study, we propose to make use of the eddy-permitting (Wekerle et al., 2017, Figure S1 in Supporting Information S1) coupled ocean general circulation—biogeochemical model (FESOM1.4-REcoM2; Schourup-Kristensen et al., 2018; Wang et al., 2018) to quantify DIN advective fluxes in the CAO. With a pan-Arctic horizontal resolution of 4.5 km, this set-up has the highest Arctic horizontal resolution of any existing global biogeochemical setup at present time. The manuscript will be presented using a bio-regional approach to consider geographic specificities of the CAO (Figure 1c) and follows a classic organization. We will first depict data and methods in Section 2. In the result Section 3, we will qualitatively and quantitatively investigate advective DIN fluxes at different spatial scales, from synoptic to sub-mesoscale, and compare their contributions. Results will be interpreted in the discussion Section 4.

2. Data and Methods

2.1. Model Description and Simulation Set-Up

Here, we used the Finite Element Sea-ice Ocean Model (FESOM) version 1.4 (Wang et al., 2014) coupled to the biogeochemical model REcoM2 (Hauck et al., 2013; Schourup-Kristensen et al., 2014). We used the same simulation that has been already extensively described and evaluated in (Schourup-Kristensen et al., 2018). The authors demonstrated the good performance of the model in terms of ocean dynamics, sea ice, light fields, nutrient concentrations and NPP.

Finite Element Sea-ice Ocean Model is a global sea-ice ocean model, which solves the primitive equations under the commonly applied Boussinesq approximations using the finite element method. The biogeochemical model REcoM2 was originally developed by Schartau et al. (2007) for mesocosm studies, and has since been further developed for large scale studies and coupled to FESOM (Schourup-Kristensen et al., 2014). In our setup, REcoM2 describes one class of zooplankton, two classes of phytoplankton, the nutrients nitrogen, silicon and iron, as well as the carbon cycle. A full description of REcoM2 can be found in Schourup-Kristensen et al. (2014) and Hauck et al. (2013).

This FESOM1.4-RECOM2 global simulation is characterized by an increased horizontal resolution of 4.5 km north of 60°N (Figure 1c). This resolution could be seen as eddy-resolving in the deepest parts of the CAO (Figure S1 in Supporting Information S1), but because it is not everywhere the case and because it does not resolve the smallest eddies (O (10 km)), we will further consider it as eddy-permitting. The resolution decreases outside of the Arctic with ∼20 km between 40 and 60°N, and a nominal resolution of 1° is used south of 40°N (Figure S1 in Supporting Information S1). The simulation comprises external sources of nutrients and carbon from rivers, and aeolian deposition of nitrogen. The reader can refer to Schourup-Kristensen et al. (2018) for a detailed description.

Finite Element Sea-ice Ocean Model was forced by the Japanese reanalysis data set (Japan Meteorological Agency, JRA55, Kobayashi et al., 2015) with sea surface salinity restoring to the PHC 3.0 climatology (Steele et al., 2001) with a restoring velocity of 1.929e−6 m s^{-1}, corresponding to 50 m per 300 days. It was spun up for 40 years in a run that has been comprehensively described in Wekerle et al. (2017). The coupled model run was started in the year 1980 and ended in 2015. The production of a biogeochemical model simulation at such high resolution is extremely expensive both in terms of computational and storage resources. Because we only analyze the upper 200 m, we consider the first 5-year as a sufficient spin-up, leaving us with a 31-year time series. The temporal resolution of the model output is monthly from 1985 to 1999 and bidaily from 2000 to 2015.

Nutrient uptake limitation is described by Michaelis–Menten kinetics in the model. The Michaelis–Menten coefficient (MM) is computed as MM = [Nut]/([Nut] + K_{Nut}), with [Nut] being the nutrient concentration, and K_{Nut} a nutrient and phytoplankton dependent half-saturation constant. The light limitation is defined as the Carbon-specific photosynthesis rate divided by the maximum photosynthetic rate (Schourup-Kristensen et al., 2018). The limitation factors have values between 0 and 1 at a given time and place, and we define a factor to be limiting when it drops below 0.5 following Schourup-Kristensen et al. (2018). For the nutrient limitation terms this means that a nutrient will be counted as limiting when the water's nutrient concentration is equal to, or less than, the half saturation constant of the phytoplankton. We derived the area limited by either nutrients (DIN or DSi) or light at the end of the productive period, for the month of September.

2.2. Geographical Delimitation in "Bio-Regions"

The CAO regions can show contrasting patterns and specific dynamics. We chose to divide the CAO in 3 regions that encompassed relatively homogeneous hydrographic and ecosystem regimes. We considered two basins (deeper than 800 m) separated by the Lomonosov ridge: the Eurasian basin (EB) and the Amerasian basin (AB), according to the bio-regionalization defined by Spalding et al. (2012). Additionally, we distinguished the pan-Arctic continental slope (SL; Figure 1c). The pan-Arctic continental slope differs from the basins and corresponds to the sharp bathymetric gradient region between 300 and 800 m isobaths (Bluhm et al., 2020). We selected latitudes greater than 66°N but we excluded the slope in the Fram Strait and Baffin Bay area (80°W–20°E, 66°N–80°N).

2.3. Calculation of Indicators for the Physical Environment

The Mixed Layer Depth (MLD), which is also the upper halocline boundary, is defined by a change in water density relative to the ocean surface of 0.125 kgm^{-3}, following Peralta-Ferriz and Woodgate (2015). The depth of the lower halocline boundary is calculated following Bourgain and Gascard (2011) where it was argued that the density ratio R_ρ may be used to mark the depth of the halocline base:

$$R_\rho = \frac{\alpha \frac{\partial \theta}{\partial z}}{\beta \frac{\partial S}{\partial z}} = 0.05 \quad (1)$$

α is the thermal expansion coefficient and β is the haline contraction coefficient, θ is potential temperature and S is salinity. This definition assumes that oceanic layers above this level are almost entirely salt-stratified with very little contribution from temperature (as reflected in $\beta\frac{\partial S}{\partial z}$ exceeding $\alpha\frac{\partial \theta}{\partial z}$ by an order of magnitude). The halocline thickness is then defined as the difference between the base of the halocline minus the MLD.

The AO halocline is a complex layer, consisting of several different water masses and source regions (Bluhm et al., 2015). Available potential energy (APE) is a good indicator of integrated changes in overall halocline and SML strength (Polyakov et al., 2018). Available potential energy is calculated as:

$$APE = \int_{z_2}^{z_1} g(\rho - \rho_{ref}) z \, dz \tag{2}$$

where z_2 is the surface and z_1 is the depth of the halocline base, g is the gravity acceleration, ρ_{ref} is potential density at the base of the halocline, and z is depth. Note that for the calculation of vertical metrics (MLD, halocline and APE) the model profiles were linearly interpolated onto a regular 1 m resolution vertical grid.

We compute EKE by decomposing zonal and meridional velocities u and v into a monthly mean (denoted by overbar) and a deviating part (denoted by prime). The formula for time-mean EKE is then:

$$\overline{EKE} = \frac{1}{2}\overline{\left((u')^2 + (v')^2\right)} = \frac{1}{2}\overline{\left(u^2 - \overline{u}^2 + v^2 - \overline{v}^2\right)} \tag{3}$$

2.4. Reynolds Decomposition

While direct observations qualitatively showed the spatio-temporal DIN dynamics and suggested a strong role for (sub)mesoscale features, they could not quantify the actual DIN transport. To do so, we derived DIN advective fluxes for the upper 200 m, expressed as ADV (DIN) in an Eulerian framework by:

$$ADV(DIN) = -< u.\nabla(DIN) > \tag{4}$$

where the angle brackets denote yearly averages and integration over the top 200 m, DIN is the concentration of DIN, u is the 3D velocity field. We decided to integrate over the upper 200 m to encompass the transition zone from the Atlantic Water layer, through the halocline, to the surface layer for the whole studied area (see Section 3.2).

The relative contribution of the various motions to the evolution of a tracer is best illustrated in terms of the Reynolds-averaged equation. This approach allows us to separate the mean and eddying (turbulent) components of the DIN advective fluxes. Following the Reynolds averaging method, u and DIN can be decomposed into a mean component $\overline{u}$ (and $\overline{DIN}$) and a fluctuating eddy component (u' and DIN' with $\overline{u'} = 0$ and $\overline{DIN'} = 0$), which leads to:

$$ADV(DIN) = -<\overline{u}.\nabla\left(\overline{DIN}\right)> - <u'.\nabla\left(DIN'\right)> \tag{5}$$

The overbar is an operator used to separate the mean from the fluctuating component over a time scale larger than the mesoscale field. Here, we have chosen a temporal 3-month average, the maximum length of oceanic mesoscale features, knowing that 94% of eddies in our simulation have lifetimes below 30 days (Wekerle et al., 2020). Every feature shorter than 3 months is therefore considered here as turbulent. Mean advective fluxes are computed as the product of u and ∇(DIN), which have the temporal resolution of model output (1 month for the 1985–200 period and 2 days for the 2000–2015 period). Eddy fluxes are derived from bi-daily outputs (thus only for the period 2000–2015) as the difference between the total and the mean advection and therefore potentially contains the contribution of both the mesoscale and the submesoscale. We derived the horizontal fluxes along longitudes (eastward) and latitudes (northward) meaning that a positive DIN flux is oriented toward the Northeast, following the CAO cyclonic circulation.

The separation between a mean large-scale and a small-scale deviation from the mean also allows us to rationalize local or remote effects (Sub)mesoscale processes are affecting tracers on local scale but are also impacting large-

scale circulation and quantities and one should consider their feedback on the mean. Indeed, during frontolysis (i.e., the decay of a front), (sub)mesoscale turbulent energy undergoes an inverse energy cascade, merging in larger features, increasing mesoscale energy, and modifying large-scale circulation. Changes in the mean advection terms can be viewed as the remote effects of (sub)mesoscale processes, while changes in the eddy terms can be interpreted as the local effects of (sub)mesoscale processes (Lévy et al., 2012).

We also separate advective horizontal (h) and vertical (v) fluxes leading to:

$$ADV(DIN) = -<\bar{u}.\nabla h\left(\overline{DIN}\right)> - <u'.\nabla h(DIN')> - <\overline{w}.\nabla v\left(\overline{DIN}\right)> - <w'.\nabla v(N')>$$
$$ADV(DIN) = \overbrace{mean\ horizontal\ flux} + \overbrace{eddy\ horizontal\ flux} + \overbrace{mean\ vertical\ flux} + \overbrace{eddy\ vertical\ flux} \quad (6)$$

u and w are the horizontal and vertical velocity fields respectively. This distinction is important since horizontal and vertical components can encompass processes of different orders of magnitude. The spatial scales can be detected in the different slopes of the variance spectra (a Fourier transformation of the squared spatial property anomaly) of the underlying flows and the property being stirred (here DIN, e.g., Lévy et al., 2018). Oceanic velocity power spectra often exhibit power-law behavior, with spatial variance proportional to k^{-a}, where k is the wavenumber, and $^{-a}$ the spectral slope on a log–log plot. Flatter slopes (less negative, e.g., k^{-1}) indicate more variance at small scales than steeper slopes (more negative, e.g., k^{-3}, Capet et al., 2008). We compared the spatial variance of the vertical and horizontal eddy fluxes (Figure S2 in Supporting Information S1). We found that the vertical eddy flux has a spectral slope of O (k^{-1}), typical of the submesoscale, while horizontal eddy fluxes were close to spectral slopes of O (k^{-3}), that is, to the mesoscale. Submesoscale features are strongly associated with frontogenesis processes (Capet et al., 2008) and associated with intense vertical movements in the upper ocean. In this study, we will compare in space and time the contributions of each of the four advective terms of Equation 6 to the annual DIN supply that are: (a) the mean horizontal flux, (b) the eddy horizontal flux, (c) the mean vertical flux and (d) the eddy vertical flux.

3. Results

3.1. Enhanced Dynamics in a Rapidly Changing Ecosystem

In this section, we investigated model outputs to describe the changing physical environment (mixing, stratification and ocean currents). We evaluated long-term (30-year) mean state and trends of qualitative indicators of the physical drivers that could affect DIN dynamics in the CAO. That is to say the MLD (i.e., vertical mixing) and APE (strength of the Arctic halocline, i.e., stratification) for vertical entrainment, and ocean current velocities and EKE for advection.

Winter MLD generally remains shallow compared to subarctic regions because of the presence of the cold halocline underneath. The winter MLD average never exceeded ~100 m (Figure 2a), which is generally shallower than the top of the nitracline layer (Figure S3 in Supporting Information S1). The MLD showed contrasted patterns between regions. The MLD in the AB and along SL (~60/52 m respectively) was shallower than in the EB (~70 m). This contrast was also visible in the mean winter APE (Figure 2c) that showed much more energy accumulated (and therefore stronger stratification) in the AB than in the EB. The APE was particularly high in the Beaufort gyre, with the minimum in the well mixed area north of the Barents Sea in the EB along the Atlantic Water pathway. The Atlantic Water pathway turns into the Arctic boundary current which flows cyclonically around the Arctic Basin along the SL. The SL is thus a place of year-round intense EKE (Figure 3a) and oceanic circulation (Figure 3c), together with the transpolar drift, from the Laptev Sea toward Fram Strait, and the outer edges of the Beaufort gyre.

Over the 1985–2015 period, linear trend analysis (right panels of Figures 2b–2d, 3b–3d, 4, Table S1 in Supporting Information S1) identified clear and significant (p-values <0.001) changes over the entire CAO, both during the winter and the summer periods. In winter, MLD deepened almost everywhere but the deepening was more intense in the AB and SL (+0.5 and + 0.2 m $year^{-1}$ respectively, Figures 2a and 2b, 4a and 4b). In the EB, MLD remained almost unchanged in winter and shallowed in summer. The stratification (i.e., APE) increased in AB ($+2.4e^4$ J m^{-2} $year^{-1}$) while it decreased in the EB ($-1.8e^4$ J m^{-2} $year^{-1}$, Figures 2c and 2d, 4c–4d). The increase in horizontal velocities (Figures 3a and 3b, 4e and 4f) were the greatest in the SL especially in summer

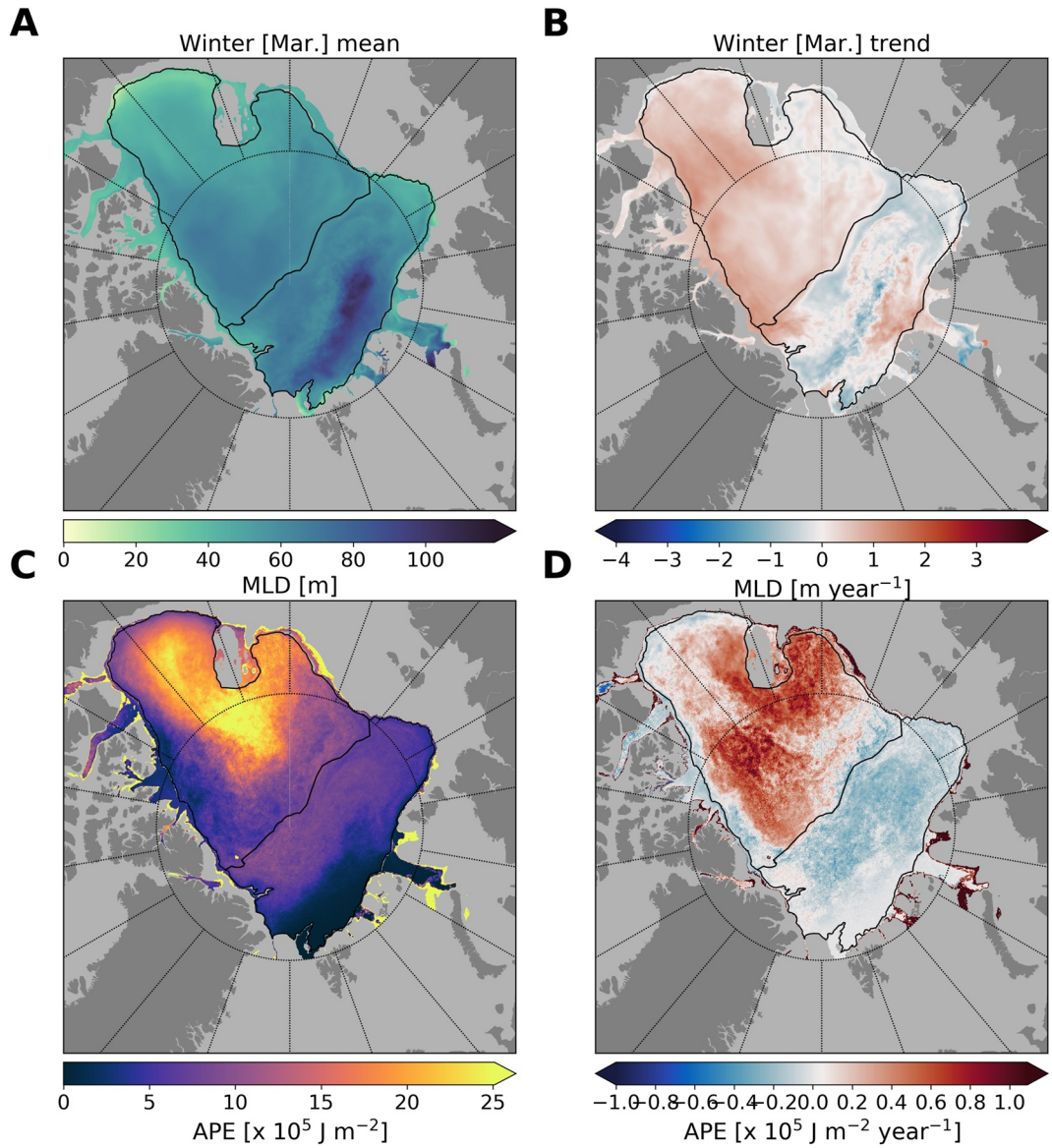

Figure 2. Winter (March) means of (a) mixed layer depth (MLD) [m] and (c) available potential energy (APE) [J m^{-2}] and their respective trends (b and d) on the right-hand side over the 1985–2015 period.

(+3.9e^{-2} cm s^{-1} year^{-1}), and to a lesser extent in the AB (+3.15e^{-2} cm s^{-1} year^{-1}), while they slightly decreased in the EB in winter (−2.5e^{-2} cm s^{-1} year^{-1}). Vertical velocities (**4G-H**) decreased almost everywhere except along the SL which showed the most positive and significant trends both in winter (+2.2e^{-2} cm s^{-1} year^{-1}) and summer (+2.4e^{-2} cm s^{-1} year^{-1}). Interestingly, an increase in EKE was found in summer in all three bio-regions but was only significant in the AB (+3.1 e^{-1} cm^2 s^{-1} year^{-1}, Figures 4i and 4j).

3.2. Imprints on DIN Transport by (Sub)Mesoscale Processes

The intensification of ocean dynamics and advective processes from mean currents to eddy activity evidenced in the previous section intuitively suggests an increasing role for DIN advection over different scales in the CAO. Here we briefly illustrate the imprint of DIN fluxes to the photic layer with daily snapshots of the model outputs (Figure 5). We chose the eastern EB which is a particularly energetic area with intense heat fluxes, eddy activity, and undergoing "Atlantification." We focused on the end of the summer productive season (5 September 2014)

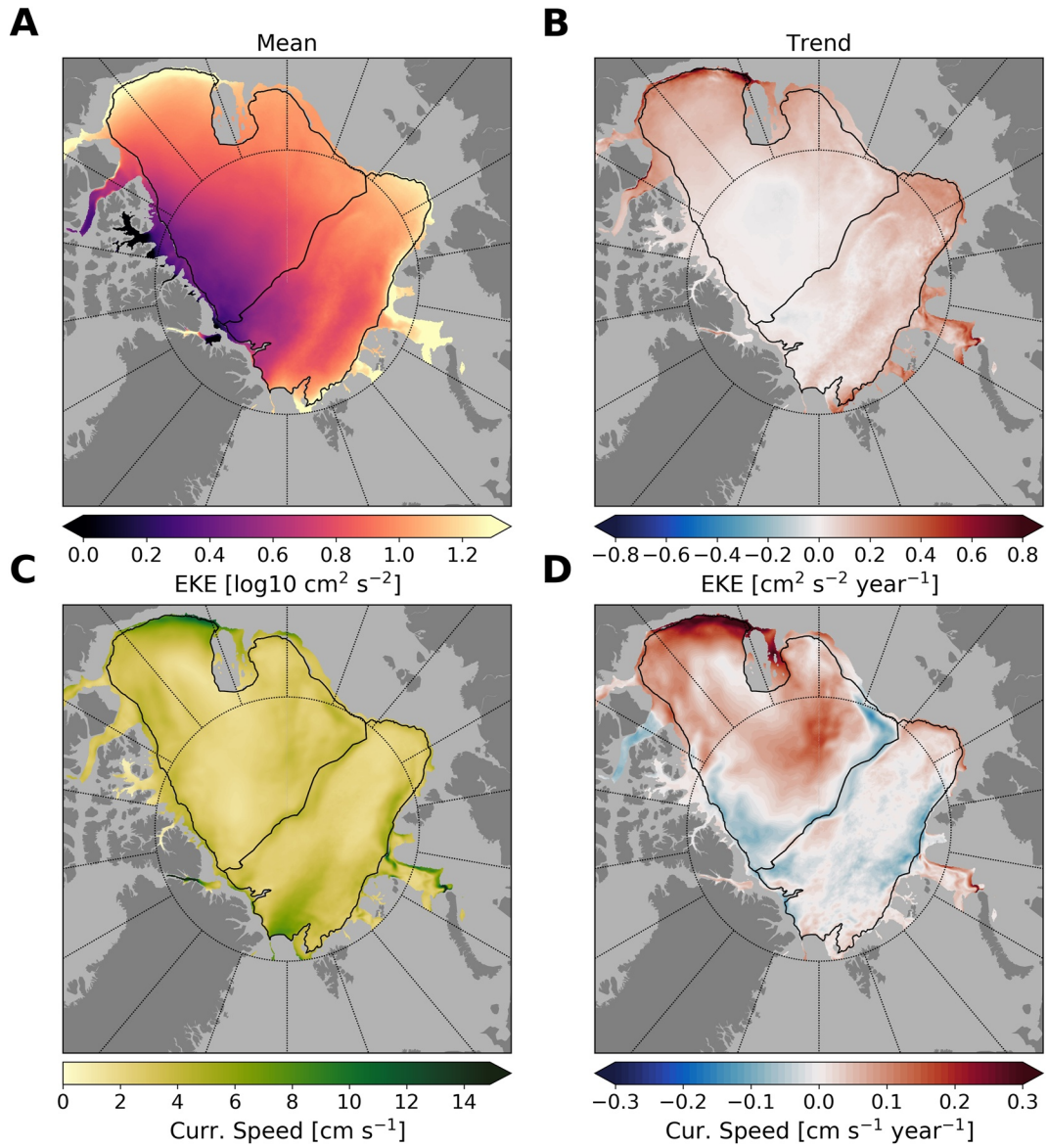

Figure 3. Annual mean of (a) eddy kinetic energy (EKE) [cm^{-2} s^{-2}] and (c) horizontal current velocities [cm s^{-1}] and their respective trends (b and d) on the right-hand side over the 1985–2015 period.

when the surface layer has been depleted by nutrient drawdown due to phytoplankton growth and is strongly nutrient-limited. The DIN supply to the surface is not directly visible because it is immediately consumed by phytoplankton. However, the daily increase in chlorophyll *a* is a good indicator of the phytoplankton growth response to the pulse of DIN supply occurring at the same time scale (Figure 5a). The area was characterized by greater than usual (sub)mesoscale activity illustrated by increased magnitude of negative and positive patches of relative vorticity (Figure 5b). A day-to-day increase in vertical velocities was also observed in the southern area where most of the chlorophyll *a* accumulation occurred (Figure 5c). Those vertical velocities are shown along a vertical section in Figure 5d and were mostly positive throughout the section. Greater magnitudes were observed close to the SL where the boundary current is flowing. The SL is a place of increasing production of (sub) mesoscale activity through the energy conversion from APE to EKE (Figure S4 in Supporting Information S1), shedding eddies and fronts toward the basin. Those features created fine scale (O (10 km)) elongated filaments of positive vertical velocities extending from the AW (~200 m), through the halocline (~150–20 m), to the surface (<20 m), providing new nutrients to the surface (Figure 5d). Note that in the interior basin, away from the slope,

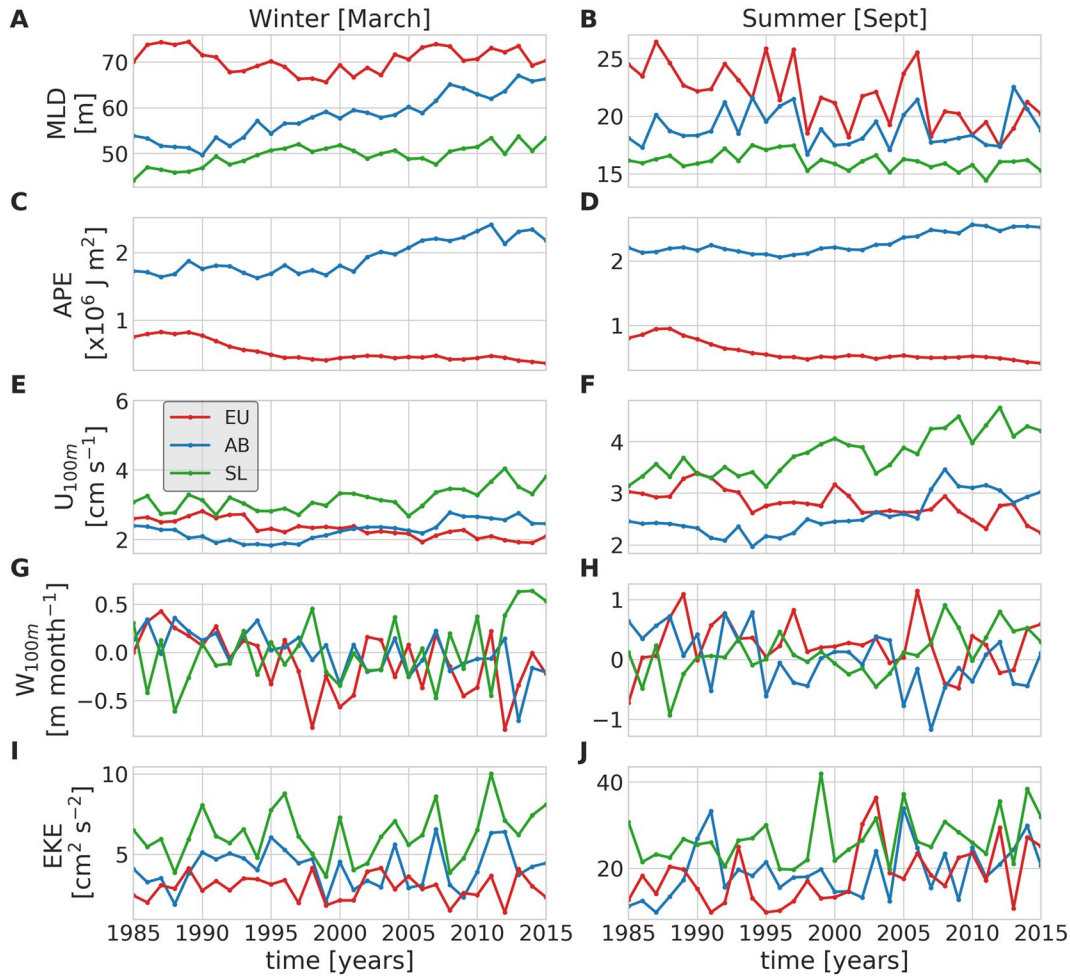

Figure 4. Time-series (1985–2015) of physical variables in winter and summer. (a and b) Mixed Layer Depth [m]; (c and d) Available Potential Energy [J m^{-2}], an indicator for the "strength" of the halocline and therefore stratification for the interior basins (SL not shown); (e and f) horizontal mean current velocities at 100 m [m s^{-1}], (g and h) vertical current velocities at 100 m [m $month^{-1}$], (i and j) Eddy Kinetic Energy [cm^2 s^{-2}].

larger scale features (consistently positive vertical velocities) suggested that atmospheric forcing may also have played a role. We showed that winds could contribute up to 45% of the upwelled water masses through Ekman pumping but that (sub)mesoscale dynamics remained the primary driver of upwelling in the EB (see Supplementary analysis 4).

3.3. Toward a DIN Budget of Advective Fluxes: Focus on (Sub)Mesoscale Processes

We quantified the contributions of each four advective terms of Equation 6 over the three bio-regions of the CAO and for the entire time series (1985–2015): the horizontal mean flux (synoptic scale), the vertical mean flux (synoptic scale), the horizontal eddy flux (mesoscale) and the vertical eddy flux (submesoscale).

The spatial distribution of the four advective terms averaged for the year 2014 are shown in Figure 6. Positive horizontal advection means a northeastward transport of DIN, while a negative horizontal advection is directed toward the southwest. Vertical advection is easier to interpret since positive (negative) means an upward (downward) transport. Overall, the magnitude of the four advective terms were by far highest along the SL and on the outer edges of the basins. Particularly strong fluxes were visible along the SL, near the Beaufort or the East-Eurasian sector, and also along the transpolar drift. Magnitudes were generally much smaller in the AB.

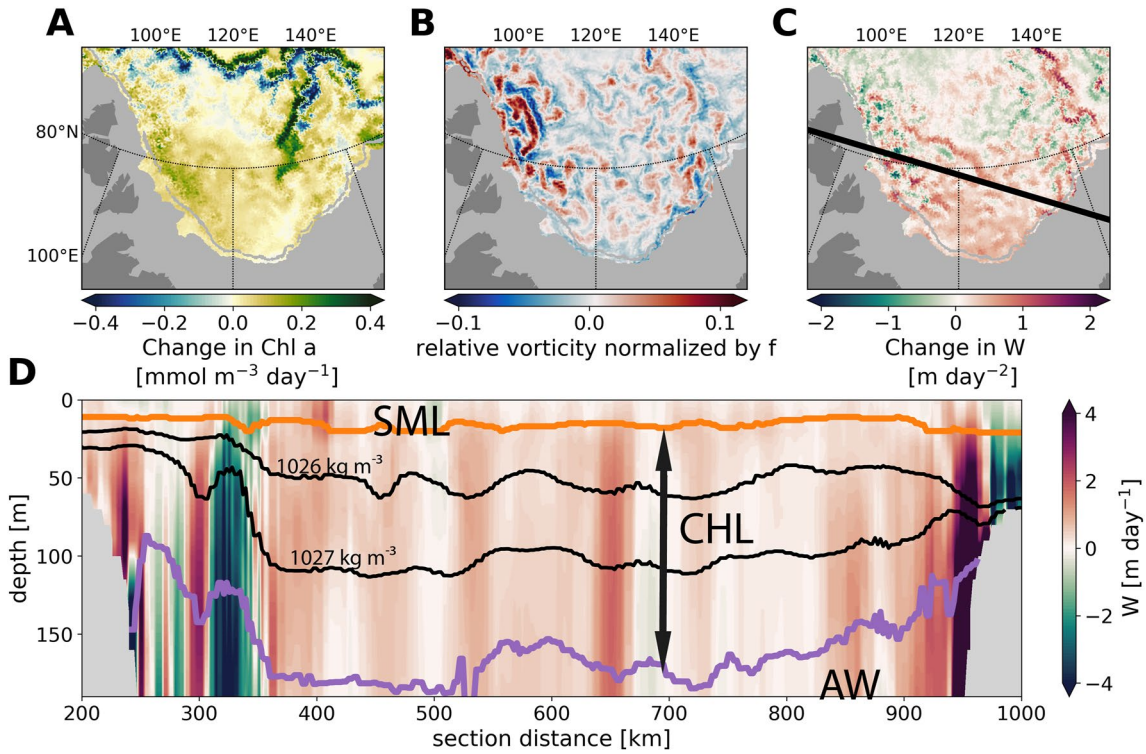

Figure 5. Illustration of (sub)mesoscale vertical advection on 5 September 2014 in the Laptev Sea, the location is marked on Figure 1C. (a) Daily change (from previous day) in surface Chlorophyll *a* [mmol m^{-3} day^{-1}], (b) surface relative vorticity normalized by *f*. (c) Daily change (from previous day) in surface vertical velocities with the black line indicating the position of the (d) vertical section of vertical velocities, with density contours (black lines, 1026 and 1027 kg m^{-3} isopycnals), mixed-layer depth (orange line) and base of the halocline (purple line, corresponding to the 0°C isotherm). Vertical velocities are stronger close to the slope and extend from the Atlantic Waters, through the cold halocline, to the surface mixed-layer. The nutrient supply results in a response of surface phytoplankton. Note that at that time, the area was ice-free.

Unsurprisingly, eddy fluxes showed very patchy features as they are associated with mesoscale and sub-mesoscale processes. The mean synoptic fluxes were also characterized by patchy features but of larger scale. This is mainly due to the time-averaging and meandering of the mean jets. The mean horizontal and vertical fluxes were similarly distributed across the study area. Positive fluxes were mostly localized in the EB and along the SL, while some negative values were present in the AB. The eddy fluxes were particularly elevated along the SL. The vertical eddy term was small away from the boundaries. The horizontal eddy flux was often composed of dipole structures. When spatially averaged for the 2000–2015 period, the total flux along the SL (1.47 mmol m^{-2} day^{-1}) is about 2 times the magnitude reached in the EB (0.73 mmol m^{-2} day^{-1}) and ∼20 times greater than those in the AB (0.08 mmol m^{-2} day^{-1}, Figure S6 in Supporting Information S1).

Time-series of yearly advective fluxes were derived by 3D integrations (spatial integration of 2D fields such as maps in Figure 6 which are already depth-integrated) and are presented in Figure 7. Note that eddy fluxes are only derived from the year 2000 and onward because it required daily fields that were only available for this period. The DIN fluxes along the SL also experienced the greatest changes with a ∼4 times increase of mean vertical transport during the 1985–2015 period (+5.4e^{9} mmol day^{-1} $year^{-1}$, $p < e^{-3}$) and a doubling of eddy horizontal transport for the 2000–2015 period (+3.1e^{10} mmol day^{-1} $year^{-1}$, $p = 3.8e^{-2}$). Mean horizontal and eddy vertical transport remained relatively constant especially in the EB where no significant trend was found (Table 1). Vertical fluxes were generally of lower magnitude than the horizontal fluxes. The mean horizontal DIN flux experienced a negative trend in the EB (−1.5e^{10} mmol day^{-1} $year^{-1}$, $p = 5e^{-3}$) especially visible for the 1985–2005 period. Another interesting feature in the EB is the dominance of the submesoscale contribution over synoptic currents for vertical DIN fluxes. The AB experienced the most decreasing trends in DIN fluxes because of the decrease in horizontal eddy and vertical mean fluxes (−2.7e^{10} mmol day^{-1} $year^{-1}$, $p = 8e^{-3}$; −1e^{10} mmol day^{-1} $year^{-1}$, $p = 5e^{-3}$). When horizontal and vertical fields were added, one should note that

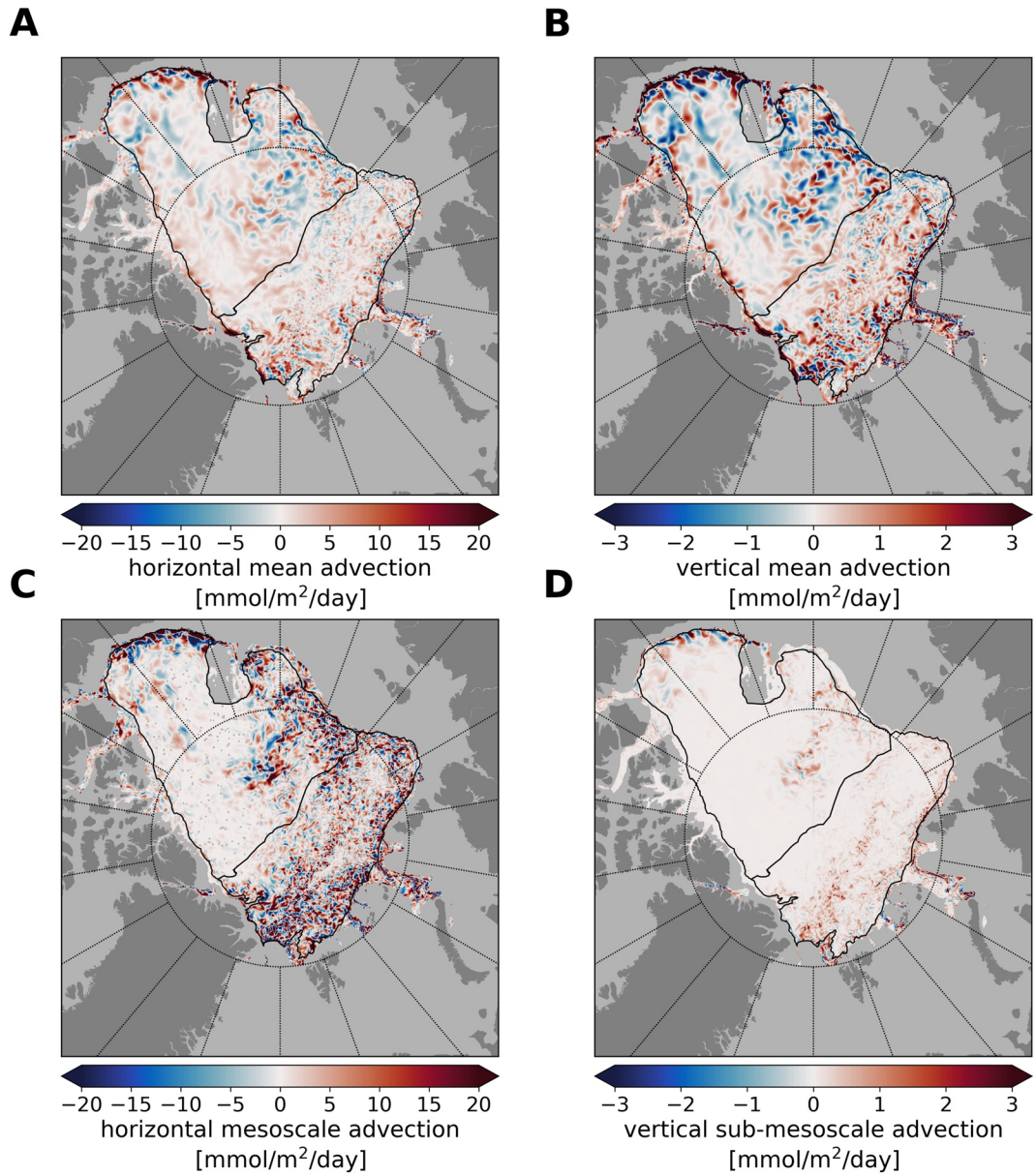

Figure 6. Annual dynamical Dissolved Inorganic Nitrogen supplies in the upper 200 m for the year 2014 from (a) horizontal mean advection (b) vertical mean advection (c) horizontal mesoscale advection and (d) vertical sub-mesoscale advection. the scale difference between horizontal (left) and vertical (right) advection.

(sub)mesoscale local processes were generally of the same order of magnitude as large-scale remote processes (Figures 7g–7i). The dominance of the SL in the total (mean + (sub)mesoscale) flux (toward the surface and the pole) accentuated from 2000 ($0.63e^{12}$ mmol day^{-1}) to 2015 ($2e^{12}$ mmol day^{-1}) compared to the EB ($0.93e^{12}$ and $1e^{12}$ mmol day^{-1} respectively) and the AB ($0.75e^{12}$ and $-0.60e^{12}$ mmol day^{-1} respectively).

4. Discussion

4.1. The Pan-Arctic Continental Slope: An Intensifying Conveyor Belt of Nutrients for the CAO Basins?

In the Arctic, the pan-Arctic continental slope (SL) dominated the magnitude of the advective nutrient fluxes compared to the interior basins (Figures 6, 7 and S6 in Supporting Information S1). Yet, the SL only occupies (~6%) of the total Arctic area (Bluhm et al., 2020). This narrow band of sharp topographic gradients therefore

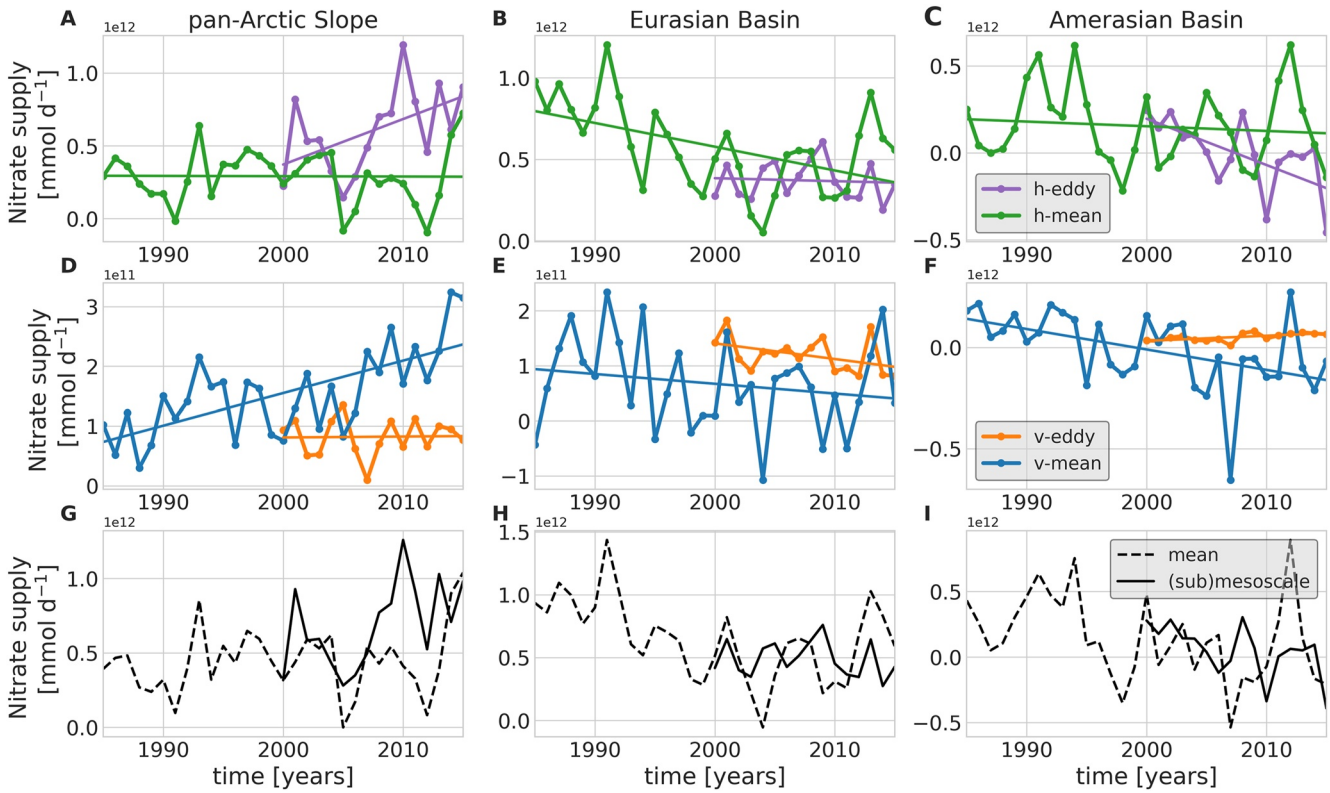

Figure 7. Interannual evolution and trend of the different advective nitrate supplies [mmol day^{-1}] integrated over space and in the upper 200 m for the three studied regions: the pan-Arctic slope (a–d–g), the Eurasian basin (b–e–h) and the AB (c–f–i). Horizontal mean (h-mean) and (sub)mesoscale (h-eddy) Dissolved Inorganic Nitrogen (DIN) advective fluxes are shown in panels (a–c); and vertical mean (v-mean) and (sub)mesoscale (v-eddy) DIN advective fluxes in panels (d–f). In the bottom panels (g–i), total (horizontal + vertical) mean and (sub)mesoscale fluxes are shown in black lines. that the y-axes scales are different in each panel.

contributes disproportionately to DIN advective fluxes given its size. One of the main characteristics of the SL is the presence of a boundary cyclonic current where inflowing Atlantic or Pacific-originated waters carry energy, heat, biomass and nutrients. An abundant literature documents the strength of those exchanges in term of heat flux (Schulz et al., 2021), zooplankton biomass (Wassmann et al., 2019), phytoplankton biomass (Oziel et al., 2020; Vernet et al., 2019), and nitrate turbulent fluxes (Randelhoff et al., 2015). The boundary current, as a jet, is also conveying kinetic energy that is eventually transferred to the mesoscale (Spall et al., 2008; Wang, Wekerle, et al., 2020). The prominent role for mesoscale eddies and submesoscale processes on shaping the AO biogeochemical environment has been documented only very recently (Schourup-Kristensen et al., 2021; Tippenhauer et al., 2021).

Results confirmed that the SL dominates total DIN supply in the CAO. It also showed that the SL was the only area that experienced an increasing trend in DIN fluxes while it decreased everywhere else in the interior basins (see next section). The DIN supply increase along the SL was mainly attributed to the increase in the horizontal mesoscale and vertical mean transport. In other terms, the increasing DIN fluxes along the SL is due to intensifying lateral eddy transport and upwelling systems. Perhaps more interestingly, the horizontal transport was dominated by the eddy field, confirming a great role for eddies to the horizontal transport of DIN from the boundary current to the basin interiors (Crews et al., 2018; Mathis et al., 2007; Watanabe et al., 2014). The Rossby radius is smaller along the SL than in the basins so that the model may not be fully resolving eddies and underestimated eddy fluxes along the SL. The increasing mean vertical advection evidences the increasing occurrence of upwelling events along the SL especially on the Pacific side. Wind-driven upwelling event were documented previously with increasing occurrence due to the loss of sea-ice and enhanced exposure to wind stress (Pickart et al., 2013).

Table 1
Statistics for Least-Squares "Two-Sided" Regressions of Annual Time Series Shown in Figures 7 and 8

Variable	Region	Slope	Intercept	*p*-value	*r*-value	Std err
h-eddy [mmol day^{-1}]	**EB**	−1.82E+09	4.02E+12	7.85E−01	−7.41E−02	6.53E+09
	AB*	−2.66E+10	5.35E+13	8.07E−03	−6.36E−01	8.63E+09
	SL*	3.13E+10	−6.22E+13	3.89E−02	5.20E−01	1.37E+10
h-mean [mmol day^{-1}]	**EB***	−1.46E+10	2.97E+13	5.11E−03	−4.90E−01	4.81E+09
	AB	−2.69E+09	5.53E+12	5.55E−01	−1.10E−01	4.50E+09
	SL	−2.07E+08	7.05E+11	9.58E−01	−9.83E−03	3.91E+09
v-eddy [mmol day^{-1}]	**EB**	−2.84E+09	5.83E+12	1.00E−01	−4.26E−01	1.62E+09
	AB*	2.56E+09	−5.08E+12	1.03E−02	6.21E−01	8.64E+08
	SL	1.56E+08	−2.31E+11	9.30E−01	2.37E−02	1.76E+09
v-mean [mmol day^{-1}]	**EB**	−1.78E+09	3.63E+12	2.97E−01	−1.94E−01	1.67E+09
	AB*	−1.01E+10	2.02E+13	5.10E−03	−4.90E−01	3.34E+09
	SL*	5.43E+09	−1.07E+13	2.64E−05	6.79E−01	1.09E+09
ANPP [TgC]	**EB***	2.04E−02	−3.99E+01	3.83E−02	0.37	9.40E−03
	AB	1.56E−02	−3.01E+01	0.16	0.26	1.09E−02
	SL*	6.58E−02	−1.29E+02	7.24E−05	0.65	1.42E−02
SIC [%]	**EB***	−1.69E−01	4.32E+02	5.24E−05	−0.66	3.57E−02
	AB*	−1.49E−01	3.91E+02	6.96E−05	−0.65	3.21E−02
	SL*	−3.66E−01	8.18E+02	3.07E−08	−0.81	4.89E−02
PAR_MLD [W m^{-2}]	**EB***	3.68E−02	−7.14E+01	9.80E−04	0.56	1.00E−02
	AB*	7.83E−02	−1.52E+02	1.08E−03	0.56	2.16E−02
	SL*	1.39E−01	−2.73E+02	7.41E−05	0.65	3.02E−02
DIN_MLD [mmol m^{-3}]	**EB***	−6.72E−02	1.38E+02	3.19E−12	−0.90	5.90E−03
	AB*	−8.29E−02	1.69E+02	1.07E−17	−0.96	4.44E−03
	SL*	−5.16E−02	1.07E+02	9.39E−15	−0.94	3.58E−03

Note. Slopes, intercept, *p*-value, *r*-value and standard error of the estimated slope. Significant regressions are identified with (*) and have *p*-values < 0.05.

4.2. Decreasing Nutrient Supply in the Interior Central Basins

The increased (mean vertical and eddy horizontal) DIN advection along the SL contrasted with the generally decreasing supply in the interior basins of the CAO. In the EB and AB, most DIN fluxes showed decreasing trends. The eddy horizontal transport in the AB showed the strongest significant decrease, followed by the mean horizontal transport in the EB and the mean vertical transport in the AB. Other fluxes trends were generally non-significant. One could however note the significant increase in vertical eddy DIN supply in the AB but its magnitude remains limited and represents a very small contribution to the total DIN supply.

The decrease in the mean vertical DIN supply in the AB is an easily predictable result given the increase in stratification driven by the freshwater accumulation in the Beaufort Gyre (Section 3.1; e.g., Rabe et al., 2011). The decreased mean horizontal DIN supply in the EB may also find a plausible explanation in the combination of (a) decreasing horizontal current velocities and (b) decreasing DIN concentrations in AW (this study, Rey. 2012). The decreasing eddy horizontal DIN transport is more surprising. In the AB, there is a small (non-significant) decrease in EKE in winter but followed by a strong (significant) increase in summer (Table S1 in Supporting Information S1). The DIN supply therefore does not follow the general increase in summer eddy activity also observed by satellite altimetry (Armitage et al., 2020). The decreased DIN supply must find an answer in weaker horizontal divergence of DIN concentrations (i.e., horizontally homogeneously distributed and depleted DIN concentrations). In a context of decreasing supply in the interior basins, the future of the productivity levels in the CAO seems to depend on the supplies carried on by the SL.

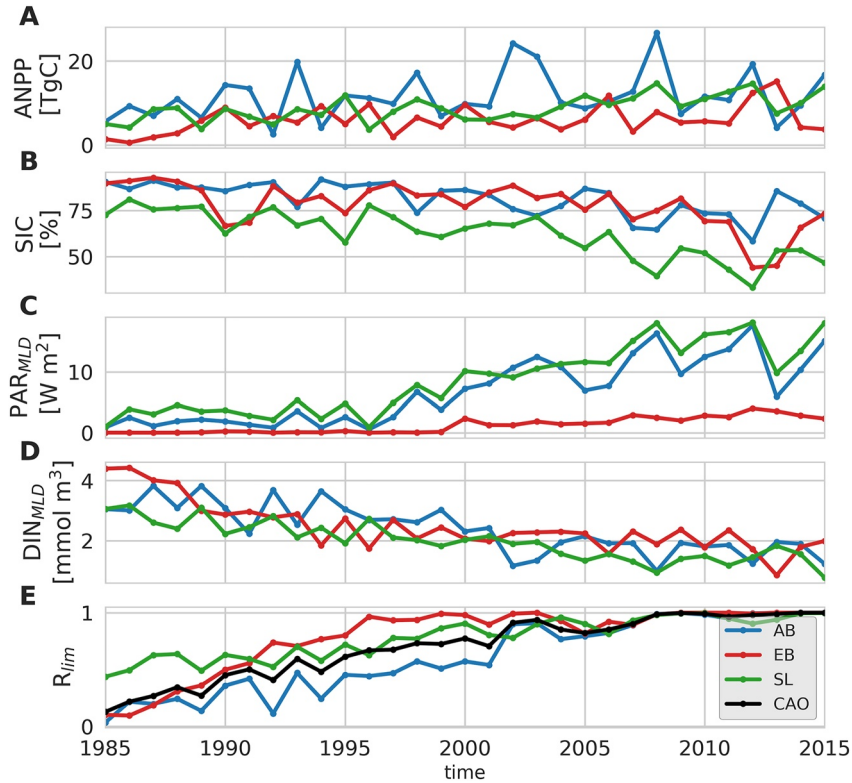

Figure 8. Time-series for the 1985–2015 period of (a) annual net primary production [TgC], (b) sea-ice concentration (%), (c) photosynthetically available radiation in the mixed layer depth (PAR_{MLD}) [W m^{-2}], (d) Dissolved Inorganic Nitrogen in the Mixed Layer Depth (DIN_{MLD}) [mmol m^{-3}], (e) Ratio of the area limited by nutrient over light in September (R_{lim}) for the 3 studied regions: Amerasian basin in blue, Eurasian basin in red and the pan-Arctic continental slope in green. The whole central Arctic Ocean is shown for R_{lim} in black line.

4.3. Increased NPP and Light Availability: A Shift Toward a Nutrient-Limited System?

The CAO experienced increasing NPP in general (Figure 8a) but the greatest absolute increase occurred in the shelves surrounding the CAO which receive nutrient inputs from land and inflowing water masses and where the sea-ice loss is the most important. This result is in agreement with recent satellite estimations (Lewis et al., 2020). Within the CAO, the SL is experiencing the steepest increase with a linear trend of +0.07 TgC $year^{-1}$ ($p < e^{-3}$, Table 1) compared with the EB (+0.02 TgC $year^{-1}$, $p < e^{-3}$) or the AB (no significant trend). This increased NPP is attributed, as expected, to a decrease in sea-ice concentration (Figure 8b) and a subsequent increase in light availability (Figure 8c). The continuous increase in NPP since 1985 has consumed more and more DIN with concentrations gradually decreasing in the surface layer (Figure 8d). The NPP increase in the CAO remains of course of lower magnitude than in the subpolar regions (Figure 9a). Although the increase remains moderate in terms of absolute NPP such as along the SL or in the eastern EB, it corresponds to the highest increase relative to the mean (Figure 9b) also corroborating satellite-derived estimations (Lewis et al., 2020). It illustrates the fast pace of the NPP changes now occurring in the CAO.

The concomitant increase in light availability and nutrient demand for phytoplankton growth has altered the limiting factors in the CAO for the last 30 years which could further be amplified by the decreasing nutrient concentrations in the inflowing AW (Rey, 2012). Based on Michaelis–Menten coefficients (see method Section 2.3), we derived the ratio of the area limited nutrients over light (R_{lim}, see Figure 8e) at the end of the summer (September). The whole CAO showed a consistent pattern toward larger (smaller) areas limited by nutrients (light) over time. The slowest changes (in the area limited by nutrients) occurred along the SL (+1.5e^{10} m^2 $year^{-1}$, $p < e^{-3}$). A change point analysis (see additional analysis 3) applied on the R_{lim} factor (Figure S7 in Supporting Information S1) showed that all three regions experienced at least two brutal changes in the mean and/or in the trend,

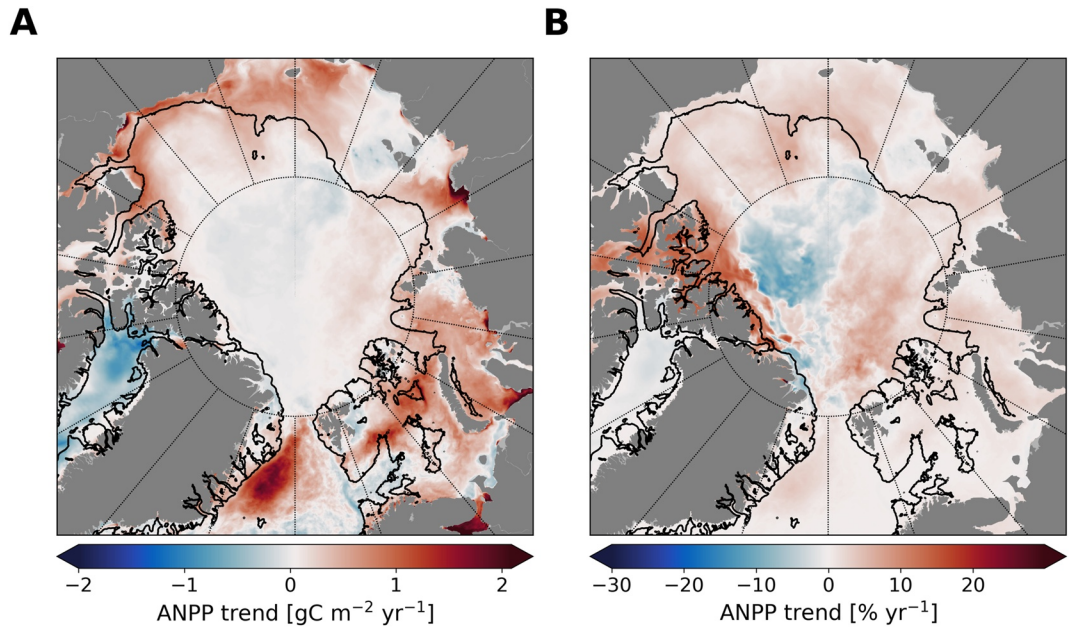

Figure 9. Absolute (a) and relative (b) linear trend (1985–2015) of annual (integrated) net primary production. Black contour indicates the 300 m isobath, the outer limits of the Central Arctic Ocean.

generally occurring during the mid-1990s and mid-2000s. It evidences that despite a quasi-linearly evolution, NPP's bottom-up control is abruptly changing.

Due to AB's physical specificity, that is, large freshwater content and stratification, DIN fluxes are extremely weak and NPP is already largely limited in nutrients. The same situation may occur in the near future in the EB where increased EKE and decreased stratification may not be sufficient to compensate for the increased nutrient drawdown by phytoplankton. The roughly constant DIN fluxes and concomitant increased primary production easily allow us to project that the system will sooner or later run into a nutrient-limited system as well, in line with recent findings based on observations (Duarte et al., 2021) or model projections (Slagstad et al., 2015). The SL, thanks to intensifying DIN fluxes, attributed to strong increase in current velocities and EKE, is also running into nutrient limitation but at a slower pace than the basins.

This study adds further evidence to the general "intensification" of ocean dynamics observed in the CAO (Section 3.1). This "intensification" of oceanic currents and (sub)mesoscale activity is either due to increased atmospheric forcing and/or buoyancy fluxes depending on the region and was also evident in observational data. For example, an intensification of near surface currents has been observed in the EB (Polyakov et al., 2020) as well as an increase of mesoscale activity in the AB (Armitage et al., 2020; Zhao et al., 2018). This "intensification" in the CAO is accompanied by increased supply and intrusions of temperate waters both from the Pacific (MacKinnon et al., 2021; Woodgate & Peralta-Ferriz, 2021) and the Atlantic gateways (Oziel et al., 2020; Wang et al., 2020). Alterations of the transpolar drift have also been reported (Krumpen et al., 2019) which could also affect the transport of shelf-derived material (Charette et al., 2020). In any case, this "intensification" increases the advective potential of nutrients, especially along the SL.

Kwiatkowski et al. (2020) still identified the AO as the ocean region most affected by nitrate limitation by the end of the century. The future levels of the CAO's productivity will therefore largely depend on the evolution of the DIN budget which could also be affected by other changing physical-biogeochemical processes. For example, warming will increase bacterial activity and potentially increase remineralization at depth and in the sediments. Sea-ice loss in summer already favors turbulent mixing in shallow areas and more resuspension of organic and inorganic material from sediments is to be expected. This process would result in tighter pelagic-benthic coupling in the adjacent shelf seas. One could also wonder whether the evolution of winter polynyas (large areas of persistent open water surrounded by sea ice) which are generally regional productive "hotspots" (Tremblay et al., 2002) will affect the CAO DIN budget. These are all pending questions that deserve to be urgently addressed by improv-

ing biogeochemical model parametrizations. Perhaps more importantly, Séférian et al. (2020) pointed out that one important limitation of current CMIP6 biogeochemical models is the lack of "comprehensive treatment of biological boundary conditions." The CAO will likely receive more and more terrigenous inputs both from rivers and erosion whereas our simulation, as most "state-of-the-art" CMIP6 biogeochemical models, only accounts for climatological riverine inputs. In our future developments, we plan for example, to develop riverine and erosion inputs dynamically coupled with the physical model.

5. Conclusions

In this study, we evaluated advective nitrate fluxes in the central Arctic Ocean (CAO) using an eddy-permitting biogeochemical model simulation during the 1985–2015 period. We performed a Reynolds decomposition to assess separately the role of synoptic current, mesoscale activity and sub-mesoscale features among the three main regions of the CAO which are the EB, the AB and the pan-Arctic continental slope. We found a major role for the pan-Arctic continental slope on the nitrate supply to the CAO. The nutrient fluxes along the pan-Arctic slope were (a) dominating the CAO fluxes, (b) experiencing strong and significant increasing trend, (c) dominated by lateral (sub)mesoscale eddy transport and mean upwelling. Despite increasing ocean dynamics, we found nitrate fluxes did not increase in the interior basins, away from the slope, and even decreased in both the Eurasian and Amerasian basins. As a result, the CAO is inexorably shifting from a light-limited to a nutrient-limited system. This situation might change in the future with altered biogeochemical cycles and increasing terrigenous inputs.

Data Availability Statement

Curated and post-processed data from FESOM1.4-REcoM2 model outputs used in this study are available at: https://doi.org/10.5281/zenodo.6448979.

Acknowledgments
This work has received funding from the European Union's Horizon 2020 research and innovation programme under grant agreement no. 820989 (project COMFORT, Our common future ocean in the Earth system –quantifying coupled cycles of carbon, oxygen, and nutrients for determining and achieving safe operating spaces with respect to tipping points) and from the Initiative and Networking Fund of the Helmholtz Association (Helmholtz Young Investigator Group Marine Carbon and Ecosystem Feedbacks in the Earth System [MarESys], Grant No. VH-NG-1301). V. Schourup-Kristensen and C. Wekerle were funded by the Frontiers in Arctic marine Monitoring program (FRAM). Computational resources were made available by the Norddeutscher Verbund für Hoch-und Höchstleistungsrechnen (HLRN). The work reflects only the authors' view; the European Commission and their executive agency are not responsible for any use that may be made of the information the work contains. The authors acknowledge support by the Open Access Publication Funds of Alfred–Wegene–Insitut Helmholtz–Zentrum für Polar– und Meeresforshung. Open access funding enabled and organized by Projekt DEAL.

References

Armitage, T. W. K., Manucharyan, G. E., Petty, A. A., Kwok, R., & Thompson, A. F. (2020). Enhanced eddy activity in the Beaufort Gyre in response to sea ice loss. *Nature Communications*, *11*(1), 1–8. https://doi.org/10.1038/s41467-020-14449-z

Arrigo, K. R., Perovich, D. K., Pickart, R. S., Brown, Z. W., Van Dijken, G. L., Lowry, K. E., et al. (2012). Massive phytoplankton blooms under Arctic sea ice. *Science*, *336*(6087), 1408. https://doi.org/10.1126/science.1215065

Arrigo, K. R., van Dijken, G., & Pabi, S. (2008). Impact of a shrinking Arctic ice cover on marine primary production. *Geophysical Research Letters*, *35*(19), 1–6. https://doi.org/10.1029/2008GL035028

Arrigo, K. R., Van Dijken, G. L., & Strong, A. L. (2015). Environmental controls of marine productivity hot spots around Antarctica. *Journal of Geophysical Research: Oceans*, *120*(8), 5545–5565. https://doi.org/10.1002/2015JC010888

Babin, M. (2020). Climate change tweaks Arctic marine ecosystems. *Science*, *369*(6500), 137–138. https://doi.org/10.1126/science.abd1231

Bluhm, B. A., Janout, M. A., Danielson, S. L., Ellingsen, I., Gavrilo, M., Grebmeier, J. M., et al. (2020). The Pan-Arctic continental slope: Sharp gradients of physical processes affect pelagic and benthic ecosystems. *Frontiers in Marine Science*, *7*, 1–25. https://doi.org/10.3389/fmars.2020.544386

Bluhm, B. A., Kosobokova, K. N., & Carmack, E. C. (2015). A tale of two basins: An integrated physical and biological perspective of the deep Arctic Ocean. *Progress in Oceanography*, *139*, 89–121. https://doi.org/10.1016/J.POCEAN.2015.07.011

Bourgain, P., & Gascard, J. C. (2011). The Arctic Ocean halocline and its interannual variability from 1997 to 2008. *Deep-Sea Research Part I Oceanographic Research Papers*, *58*(7), 745–756. https://doi.org/10.1016/j.dsr.2011.05.001

Brown, K. A., Holding, J. M., & Carmack, E. C. (2020). Understanding regional and seasonal variability is key to gaining a Pan-Arctic perspective on Arctic Ocean freshening. *Frontiers in Marine Science*, *7*, 1–25. https://doi.org/10.3389/fmars.2020.00606

Capet, X., McWilliams, J. C., Molemaker, M. J., & Shchepetkin, A. F. (2008). Mesoscale to submesoscale transition in the California Current system. Part I: Flow structure, eddy flux, and observational tests. *Journal of Physical Oceanography*, *38*(1), 29–43. https://doi.org/10.1175/2007JPO3671.1

Carmack, E., & Wassmann, P. (2006). Food webs and physical-biological coupling on pan-Arctic shelves: Unifying concepts and comprehensive perspectives. *Progress in Oceanography*, *71*(2–4), 446–477. https://doi.org/10.1016/j.pocean.2006.10.004

Carmack, E. C., Yamamoto-Kawai, M., Haine, T. W. N., Bacon, S., Bluhm, B. A., Lique, C., et al. (2016). Freshwater and its role in the Arctic Marine System: Sources, disposition, storage, export, and physical and biogeochemical consequences in the Arctic and global oceans. *Journal of Geophysical Research: Biogeosciences*, *121*(3), 675–717. https://doi.org/10.1002/2015JG003140

Charette, M. A., Kipp, L. E., Jensen, L. T., Dabrowski, J. S., Whitmore, L. M., Fitzsimmons, J. N., et al. (2020). The transpolar drift as a source of riverine and shelf-derived trace elements to the central Arctic Ocean. *Journal of Geophysical Research: Oceans*, *125*(5), 1–34. https://doi.org/10.1029/2019JC015920

Codispoti, L. A., Kelly, V., Thessen, A., Matrai, P., Suttles, S., Hill, V., et al. (2013). Synthesis of primary production in the Arctic Ocean: III. Nitrate and phosphate based estimates of net community production. *Progress in Oceanography*, *110*(2012), 126–150. https://doi.org/10.1016/j.pocean.2012.11.006

Crews, L., Sundfjord, A., Albretsen, J., & Hattermann, T. (2018). Mesoscale eddy activity and transport in the Atlantic Water inflow region north of svalbard. *Journal of Geophysical Research: Oceans*, *123*(1), 201–215. https://doi.org/10.1002/2017JC013198

D'Asaro, E. A., & Morison, J. H. (1992). Internal waves and mixing in the Arctic Ocean. *Deep-Sea Research Part A, Oceanographic Research Papers*, *39*(2), S459–S484. https://doi.org/10.1016/S0198-0149(06)80016-6

D'Ovidio, F., De Monte, S., Alvain, S., Dandonneau, Y., & Lévy, M. (2010). Fluid dynamical niches of phytoplankton types. *Proceedings of the National Academy of Sciences of the United States of America*, *107*(43), 18366–18370. https://doi.org/10.1073/pnas.1004620107

Duarte, P., Meyer, A., & Moreau, S. (2021). Nutrients in water masses in the Atlantic sector of the Arctic Ocean: Temporal trends, mixing and links with primary production. *Journal of Geophysical Research: Oceans*, *126*(8). https://doi.org/10.1029/2021jc017413

Hauck, J., Völker, C., Wang, T., Hoppema, M., Losch, M., & Wolf-Gladrow, D. A. (2013). Seasonally different carbon flux changes in the Southern Ocean in response to the southern annular mode. *Global Biogeochemical Cycles*, *27*(4), 1236–1245. https://doi.org/10.1002/2013GB004600

Hunt, G. L., Drinkwater, K. F., Arrigo, K., Berge, J., Daly, K. L., Danielson, S., et al. (2016). Advection in polar and sub-polar environments: Impacts on high latitude marine ecosystems. *Progress in Oceanography*, *149*, 40–81. https://doi.org/10.1016/j.pocean.2016.10.004

Ingvaldsen, R. B., Assmann, K. M., Primicerio, R., Fossheim, M., Polyakov, I. V., & Dolgov, A. V. (2021). Physical manifestations and ecological implications of Arctic Atlantification. *Nature Reviews Earth & Environment*, 0123456789. https://doi.org/10.1038/s43017-021-00228-x

Kobayashi, S., Ota, Y., Harada, Y., Ebita, A., Moriya, M., Onoda, H., et al. (2015). The JRA-55 reanalysis: General specifications and basic characteristics. *Journal of the Meteorological Society of Japan*, *93*(1), 5–48. https://doi.org/10.2151/jmsj.2015-001

Krumpen, T., Belter, H. J., Boetius, A., Damm, E., Haas, C., Hendricks, S., et al. (2019). Arctic warming interrupts the Transpolar Drift and affects long-range transport of sea ice and ice-rafted matter. *Scientific Reports*, *9*(1), 1–9. https://doi.org/10.1038/s41598-019-41456-y

Kwiatkowski, L., Torres, O., Bopp, L., Aumont, O., Chamberlain, M., Christian, J., et al. (2020). Twenty-first century ocean warming, acidification, deoxygenation, and upper ocean nutrient decline from CMIP6 model projections. *Biogeosciences Discussions*, 1–43. https://doi.org/10.5194/bg-2020-16

Kwok, R. (2018). Arctic sea ice thickness, volume, and multiyear ice coverage: Losses and coupled variability (1958–2018). *Environmental Research Letters*, *13*(10), 105005. https://doi.org/10.1088/1748-9326/aae3ec

Lévy, M. (2008). The modulation of biological production by oceanic mesoscale turbulence. *Lecture Notes in Physics*, *744*, 219–261. https://doi.org/10.1007/978-3-540-75215-8_9

Lévy, M., Franks, P. J. S., & Smith, K. S. (2018). The role of submesoscale currents in structuring marine ecosystems. *Nature Communications*, *9*(1), 4758. https://doi.org/10.1038/s41467-018-07059-3

Lévy, M., Iovino, D., Resplandy, L., Klein, P., Madec, G., Tréguier, A. M., et al. (2012). Large-scale impacts of submesoscale dynamics on phytoplankton: Local and remote effects. *Ocean Modelling*, *43*(44), 77–93. https://doi.org/10.1016/j.ocemod.2011.12.003

Lewis, K. M., Van Dijken, G. L., & Arrigo, K. R. (2020). Changes in phytoplankton concentration now drive increased Arctic Ocean primary production. *Science*, *369*(6500), 198–202. https://doi.org/10.1126/science.aay8380

Li, W. K. W., McLaughlin, F. A., Lovejoy, C., & Carmack, E. C. (2009). Smallest algae thrive as the Arctic Ocean freshens. *Science*, *326*(5952), 539. https://doi.org/10.1126/science.1179798

Lin, P., Pickart, R. S., McRaven, L. T., Arrigo, K. R., Bahr, F., Lowry, K. E., et al. (2019). Water mass evolution and circulation of the northeastern Chukchi Sea in summer: Implications for nutrient distributions. *Journal of Geophysical Research: Oceans*, *124*(7), 4416–4432. https://doi.org/10.1029/2019JC015185

Lind, S., Ingvaldsen, R. B., & Furevik, T. (2018). Arctic warming hotspot in the northern Barents Sea linked to declining sea-ice import. *Nature Climate Change*, *8*(7), 634–639. https://doi.org/10.1038/s41558-018-0205-y

MacKinnon, J. A., Simmons, H. L., Hargrove, J., Thomson, J., Peacock, T., Alford, M. H., et al. (2021). A warm jet in a cold ocean. *Nature Communications*, *12*(1), 1–12. https://doi.org/10.1038/s41467-021-22505-5

Mathis, J. T., Pickart, R. S., Hansell, D. A., Kadko, D., & Bates, N. R. (2007). Eddy transport of organic carbon and nutrients from the Chukchi Shelf: Impact on the upper halocline of the Western Arctic Ocean. *Journal of Geophysical Research*, *112*(5), 1–14. https://doi.org/10.1029/2006JC003899

Meneghello, G., Marshall, J., Timmermans, M. L., & Scott, J. (2018). Observations of seasonal upwelling and downwelling in the Beaufort Sea mediated by sea ice. *Journal of Physical Oceanography*, *48*(4), 795–805. https://doi.org/10.1175/JPO-D-17-0188.1

Nicolaus, M., Katlein, C., Maslanik, J., & Hendricks, S. (2012). Changes in Arctic sea ice result in increasing light transmittance and absorption. *Geophysical Research Letters*, *39*(24), 1–6. https://doi.org/10.1029/2012GL053738

Oziel, L., Baudena, A., Ardyna, M., Massicotte, P., Randelhoff, A., Sallée, J. B., et al. (2020). Faster Atlantic currents drive poleward expansion of temperate phytoplankton in the Arctic Ocean. *Nature Communications*, *11*(1), 1–8. https://doi.org/10.1038/s41467-020-15485-5

Peralta-Ferriz, C., & Woodgate, R. A. (2015). Seasonal and interannual variability of pan-Arctic surface mixed layer properties from 1979 to 2012 from hydrographic data, and the dominance of stratification for multiyear mixed layer depth shoaling. *Progress in Oceanography*, *134*, 19–53. https://doi.org/10.1016/j.pocean.2014.12.005

Pickart, R. S., Schulze, L. M., Moore, G. W. K., Charette, M. A., Arrigo, K. R., van Dijken, G., & Danielson, S. L. (2013). Long-term trends of upwelling and impacts on primary productivity in the Alaskan Beaufort Sea. *Deep-Sea Research Part I Oceanographic Research Papers*, *79*, 106–121. https://doi.org/10.1016/j.dsr.2013.05.003

Pnyushkov, A. V., Polyakov, I. V., Rember, R., Ivanov, V. V., Alkire, M. B., Ashik, I. M., et al. (2018). Heat, salt, and volume transports in the eastern Eurasian Basin of the Arctic Ocean from 2 years of mooring observations. *Ocean Science*, *14*(6), 1349–1371. https://doi.org/10.5194/os-14-1349-2018

Polyakov, I. V., Pnyushkov, A. V., Alkire, M. B., Ashik, I. M., Baumann, T. M., Carmack, E. C., et al. (2017). Greater role for Atlantic inflows on Sea-ice loss in the Eurasian basin of the Arctic Ocean. *Science*, *356*(6335), 285–291. https://doi.org/10.1126/science.aai8204

Polyakov, I. V., Pnyushkov, A. V., & Carmack, E. C. (2018). Stability of the arctic halocline: A new indicator of Arctic climate change. *Environmental Research Letters*, *13*(12), 125008. https://doi.org/10.1088/1748-9326/aaec1e

Polyakov, I. V., Rippeth, T. P., Fer, I., Baumann, T. M., Carmack, E. C., Ivanov, V. V., et al. (2020). Intensification of near-surface currents and shear in the eastern Arctic Ocean. *Geophysical Research Letters*, *47*(16), 1–9. https://doi.org/10.1029/2020GL089469

Popova, E. E., Yool, A., Aksenov, Y., & Coward, A. C. (2013). Role of advection in Arctic Ocean lower trophic dynamics: A modeling perspective. *Journal of Geophysical Research: Oceans*, *118*(3), 1571–1586. https://doi.org/10.1002/jgrc.20126

Rabe, B., Karcher, M., Kauker, F., Schauer, U., Toole, J. M., Krishfield, R. A., et al. (2014). Arctic Ocean basin liquid freshwater storage trend 1992–2012. *Geophysical Research Letters*, *41*(3), 961–968. https://doi.org/10.1002/2013GL058121

Rabe, B., Karcher, M., Schauer, U., Toole, J. M., Krishfield, R. A., Pisarev, S., et al. (2011). An assessment of Arctic Ocean freshwater content changes from the 1990s to the 2006–2008 period. *Deep-Sea Research I*, *58*(2), 173–185. https://doi.org/10.1016/j.dsr.2010.12.002

Rainville, L., Lee, C. M., & Woodgate, R. A. (2011). Impact of wind-driven mixing in the Arctic Ocean. *Oceanography*, *24*(3), 136–145. https://doi.org/10.5670/oceanog.2011.65

Rainville, L., & Winsor, P. (2008). Mixing across the Arctic Ocean: Microstructure observations during the Beringia 2005 expedition. *Geophysical Research Letters*, *35*(8), 2–6. https://doi.org/10.1029/2008GL033532

Randelhoff, A., Fer, I., & Sundfjord, A. (2017). Turbulent upper-ocean mixing affected by meltwater layers during Arctic summer. *Journal of Physical Oceanography*, *47*(4), 835–853. https://doi.org/10.1175/JPO-D-16-0200.1

Randelhoff, A., Holding, J., Janout, M., Sejr, M. K., Babin, M., Tremblay, J. É., & Alkire, M. B. (2020). Pan-Arctic Ocean primary production constrained by turbulent nitrate fluxes. *Frontiers in Marine Science*, *7*, 1–15. https://doi.org/10.3389/fmars.2020.00150

Randelhoff, A., Reigstad, M., Chierici, M., Sundfjord, A., Ivanov, V., Cape, M., et al. (2018). Seasonality of the physical and biogeochemical hydrography in the inflow to the Arctic Ocean through Fram Strait. *Frontiers in Marine Science*, *5*, 1–16. https://doi.org/10.3389/fmars.2018.00224

Randelhoff, A., Sundfjord, A., & Reigstad, M. (2015). Seasonal variability and fluxes of nitrate in the surface waters over the Arctic shelf slope. *Geophysical Research Letters*, *42*(9), 3442–3449. https://doi.org/10.1002/2015GL063655

Rey, F. (2012). Declining silicate concentrations in the Norwegian and Barents seas. *ICES Journal of Marine Science*, *69*(2), 208–212. https://doi.org/10.1093/icesjms/fss007

Rippeth, T. P., Lincoln, B. J., Lenn, Y. D., Green, J. A. M., Sundfjord, A., & Bacon, S. (2015). Tide-mediated warming of Arctic halocline by Atlantic heat fluxes over rough topography. *Nature Geoscience*, *8*(3), 191–194. https://doi.org/10.1038/ngeo2350

Schartau, M., Engel, A., Schröter, J., Thoms, S., Völker, C., & Wolf-Gladrow, D. (2007). Modelling carbon overconsumption and the formation of extracellular particulate organic carbon. *Biogeosciences Discussions*, *4*(1), 13–67. https://doi.org/10.5194/bgd-4-13-2007

Schourup-Kristensen, V., Sidorenko, D., Wolf-Gladrow, D. A., & Völker, C. (2014). A skill assessment of the biogeochemical model REcoM2 coupled to the Finite Element Sea Ice-Ocean Model (FESOM 1.3). *Geoscientific Model Development*, *7*(6), 2769–2802. https://doi.org/10.5194/gmd-7-2769-2014

Schourup-Kristensen, V., Wekerle, C., Danilov, S., & Völker, C. (2021). Seasonality of mesoscale phytoplankton control in eastern Fram Strait. *Journal of Geophysical Research: Oceans*, *126*(10), 1–24. https://doi.org/10.1029/2021jc017279

Schourup-Kristensen, V., Wekerle, C., Wolf-Gladrow, D. A., & Völker, C. (2018). Arctic Ocean biogeochemistry in the high resolution FESOM 1.4-REcoM2 model. *Progress in Oceanography*, *168*, 65–81. https://doi.org/10.1016/j.pocean.2018.09.006

Schulz, K., Janout, M., Lenn, Y. D., Ruiz-Castillo, E., Polyakov, I., Mohrholz, V., et al. (2021). On the along-slope heat loss of the boundary current in the eastern Arctic Ocean. *Journal of Geophysical Research: Oceans*, *126*(2). https://doi.org/10.1029/2020JC016375

Séférian, R., Berthet, S., Yool, A., Palmiéri, J., Bopp, L., Tagliabue, A., et al. (2020). Tracking improvement in simulated marine biogeochemistry between CMIP5 and CMIP6. *Current Climate Change Reports*, *6*(3), 95–119. https://doi.org/10.1007/s40641-020-00160-0

Serreze, M. C., & Meier, W. N. (2019). The Arctic's Sea ice cover: Trends, variability, predictability, and comparisons to the Antarctic. *Annals of the New York Academy of Sciences*, *1436*(1), 36–53. https://doi.org/10.1111/nyas.13856

Sévigny, C., Gratton, Y., & Galbraith, P. S. (2015). Frontal structures associated with coastal upwelling and ice-edge subduction events in southern Beaufort Sea during the Canadian Arctic Shelf Exchange Study. *Journal of Geophysical Research: Oceans*, *120*(4), 2523–2539. https://doi.org/10.1002/2014JC010641

Sigmond, M., Fyfe, J. C., & Swart, N. C. (2018). Ice-free Arctic projections under the Paris agreement. *Nature Climate Change*, *8*(5), 404–408. https://doi.org/10.1038/s41558-018-0124-y

Slagstad, D., Wassmann, P. F. J., & Ellingsen, I. (2015). Physical constrains and productivity in the future Arctic Ocean. *Frontiers in Marine Science*, *2*, 1–23. https://doi.org/10.3389/fmars.2015.00085

Spalding, M. D., Agostini, V. N., Rice, J., & Grant, S. M. (2012). Pelagic provinces of the world: A biogeographic classification of the world's surface pelagic waters. *Ocean & Coastal Management*, *60*, 19–30. https://doi.org/10.1016/j.ocecoaman.2011.12.016

Spall, M. A., Pickart, R. S., Brugler, E. T., Moore, G. W. K., Thomas, L., & Arrigo, K. R. (2014). Role of shelfbreak upwelling in the formation of a massive under-ice bloom in the Chukchi Sea. *Deep Sea Research Part II: Topical Studies in Oceanography*, *105*, 17–29. https://doi.org/10.1016/j.dsr2.2014.03.017

Spall, M. A., Pickart, R. S., Fratantoni, P. S., & Plueddemann, A. J. (2008). Western arctic shelfbreak eddies: Formation and transport. *Journal of Physical Oceanography*, *38*(8), 1644–1668. https://doi.org/10.1175/2007JPO3829.1

Steele, M., Morley, R., & Ermold, W. (2001). PHC: A global ocean hydrography with a high-quality Arctic Ocean. *Journal of Climate*, *14*(9), 2079–2087. https://doi.org/10.1175/1520-0442(2001)014

Stroeve, J., & Notz, D. (2018). Changing state of Arctic sea ice across all seasons. *Environmental Research Letters*, *13*(10), 103001. https://doi.org/10.1088/1748-9326/aade56

Timmermans, M. L., & Marshall, J. (2020). Understanding Arctic Ocean circulation: A review of ocean dynamics in a changing climate. *Journal of Geophysical Research: Oceans*, *125*(4), 1–70. https://doi.org/10.1029/2018JC014378

Tippenhauer, S., Janout, M., Chouksey, M., Torres-Valdes, S., Fong, A., & Wulff, T. (2021). Substantial sub-surface chlorophyll patch sustained by vertical nutrient fluxes in Fram Strait observed with an autonomous underwater vehicle. *Frontiers in Marine Science*, *8*, 1–13. https://doi.org/10.3389/fmars.2021.605225

Tremblay, J. É., Anderson, L. G., Matrai, P., Coupel, P., Bélanger, S., Michel, C., & Reigstad, M. (2015). Global and regional drivers of nutrient supply, primary production and CO2 drawdown in the changing Arctic Ocean. *Progress in Oceanography*, *139*, 171–196. https://doi.org/10.1016/j.pocean.2015.08.009

Tremblay, J. É., Gratton, Y., Carmack, E. C., Payne, C. D., & Price, N. M. (2002). Impact of the large-scale Arctic circulation and the north water polynya on nutrient inventories in Baffin Bay. *Journal of Geophysical Research*, *107*(8), 1–15. https://doi.org/10.1029/2000jc000595

Vancoppenolle, M., Meiners, K. M., Michel, C., Bopp, L., Brabant, F., Carnat, G., et al. (2013). Role of sea ice in global biogeochemical cycles: Emerging views and challenges. *Quaternary Science Reviews*, *79*, 207–230. https://doi.org/10.1016/j.quascirev.2013.04.011

Vernet, M., Ellingsen, I. H., Seuthe, L., Slagstad, D., Cape, M. R., & Matrai, P. A. (2019). Influence of phytoplankton advection on the productivity along the Atlantic water inflow to the Arctic Ocean. *Frontiers in Marine Science*, *6*, 583. https://doi.org/10.3389/fmars.2019.00583

Wang, Q., Danilov, S., Sidorenko, D., Timmermann, R., Wekerle, C., Wang, X., et al. (2014). The finite Element Sea ice-ocean model (FESOM) v.1.4: Formulation of an ocean general circulation model. *Geoscientific Model Development*, *7*(2), 663–693. https://doi.org/10.5194/gmd-7-663-2014

Wang, Q., Koldunov, N. V., Danilov, S., Sidorenko, D., Wekerle, C., Scholz, P., et al. (2020). Eddy kinetic energy in the Arctic Ocean from a global simulation with a 1-km Arctic. *Geophysical Research Letters*, *47*(14). https://doi.org/10.1029/2020GL088550

Wang, Q., Wekerle, C., Danilov, S., Wang, X., & Jung, T. (2018). A 4.5g km resolution Arctic Ocean simulation with the global multi-resolution model FESOM 1.4. *Geoscientific Model Development*, *11*(4), 1229–1255. https://doi.org/10.5194/gmd-11-1229-2018

Wang, Q., Wekerle, C., Wang, X., Danilov, S., Koldunov, N., Sein, D., et al. (2020). Intensification of the Atlantic water supply to the Arctic Ocean through Fram Strait induced by Arctic sea ice decline. *Geophysical Research Letters*, *47*(3). https://doi.org/10.1029/2019GL086682

Wassmann, P. F., Slagstad, D., & Ellingsen, I. (2019). Advection of mesozooplankton into the northern Svalbard shelf region. *Frontiers in Marine Science*, *6*, 1–10. https://doi.org/10.3389/fmars.2019.00458

Wassmann, P., Kosobokova, K. N., Slagstad, D., Drinkwater, K. F., Hopcroft, R. R., Moore, S. E., et al. (2015). The contiguous domains of Arctic Ocean advection: Trails of life and death. *Progress in Oceanography*, *139*, 42–65. https://doi.org/10.1016/j.pocean.2015.06.011

Watanabe, E., Onodera, J., Harada, N., Honda, M. C., Kimoto, K., Kikuchi, T., et al. (2014). Enhanced role of eddies in the Arctic marine biological pump. *Nature Communications*, *5*, 3950. https://doi.org/10.1038/ncomms4950

Wekerle, C., Hattermann, T., Wang, Q., Crews, L., von Appen, W.-J., & Danilov, S. (2020). Properties and dynamics of mesoscale eddies in Fram Strait from a comparison between two high-resolution ocean–sea ice models. *Ocean Science*, *16*(5), 1225–1246. https://doi.org/10.5194/os-16-1225-2020

Wekerle, C., Wang, Q., Danilov, S., Schourup-Kristensen, V., von Appen, W. J., & Jung, T. (2017). Atlantic Water in the Nordic Seas: Locally eddy-permitting ocean simulation in a global setup. *Journal of Geophysical Research: Oceans*, *122*(2), 914–940. https://doi.org/10.1002/2016JC012121

Woodgate, R. A., & Peralta-Ferriz, C. (2021). Warming and freshening of the Pacific inflow to the Arctic from 1990–2019 implying dramatic shoaling in Pacific winter water ventilation of the Arctic water column. *Geophysical Research Letters*, *48*(9). https://doi.org/10.1029/2021gl092528

Yamamoto-Kawai, M., Tanaka, N., & Pivovarov, S. (2005). Freshwater and brine behaviors in the Arctic ocean deduced from historical data of $\delta^{18}O$ and alkalinity (1929–2002 A.D.). *Journal of Geophysical Research*, *110*(10), 1–16. https://doi.org/10.1029/2004JC002793

Zhao, M., Timmermans, M. L., Krishfield, R., & Manucharyan, G. (2018). Partitioning of kinetic energy in the Arctic Ocean's Beaufort Gyre. *Journal of Geophysical Research: Oceans*, *123*(7), 4806–4819. https://doi.org/10.1029/2018JC014037